

# ChangeBridge: Spatiotemporal Image Generation with Multimodal Controls for Remote Sensing

Zhengkui Zhao  
Wuhan University

Chen Wu\*  
Wuhan University

Di Wang  
Wuhan University

Hongruixuan Chen  
University of Tokyo

Zhuo Zheng  
Stanford University

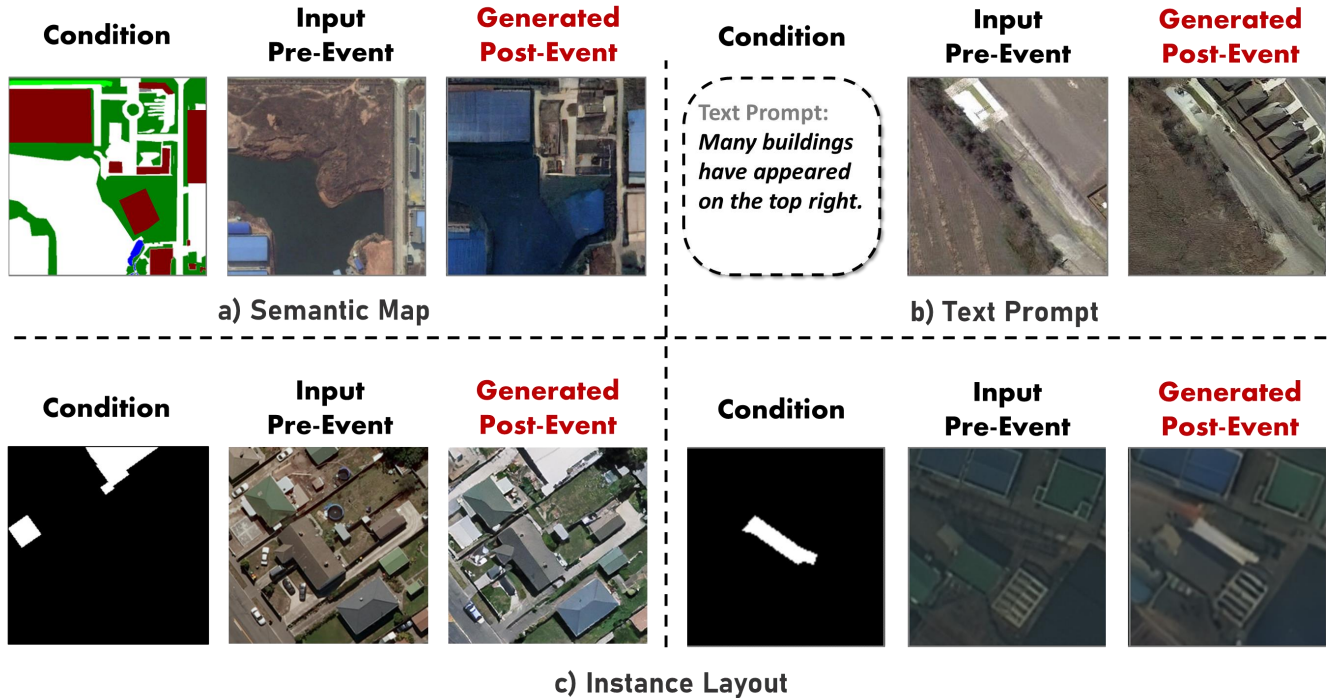


Figure 1. ChangeBridge generates post-event images from pre-event inputs, conditioned on a) semantic maps, b) text prompts, and c) instance layouts.

## Abstract

Recent advancements in generative methods, especially diffusion models, have made great progress in remote sensing image synthesis. Despite these advancements, existing methods have not explored the simulation of future scenarios based on given scenario images. This simulation capability has wide applications for urban planning, land management. ChangeBridge: Spatiotemporal Image Generation with Multimodal Controls, and beyond. In this work, we propose ChangeBridge, a conditional spatiotemporal diffusion model. Given pre-event images and conditioned on multimodal spatial controls (e.g., text prompts, instance layouts, and semantic maps), ChangeBridge can synthesize post-event images. The core idea behind ChangeBridge is to modeling the noise-to-image diffusion model, as a pre-to-post diffusion bridge. Conditioned on multimodal controls, ChangeBridge leverages a stochastic Brownian-bridge dif-

fusion, directly modeling the spatiotemporal evolution between pre-event and post-event states. To the best of our knowledge, ChangeBridge is the first spatiotemporal generative model with multimodal controls for remote sensing. Experimental results demonstrate that ChangeBridge can simulate high-fidelity future scenarios aligned with given conditions, including event and event-driven background variations. Code will be available.

## 1. Introduction

Remote-sensing generation methods have significantly advanced by diffusion models as the mainstream generative technique. These advanced methods include layout-to-image synthesis [1, 42], modality transfer [5, 19], resolution modification [41, 48], and text-to-image generation [15, 31]. However, despite the diversity of these generative approaches, a key challenge remains: synthesizing fu-

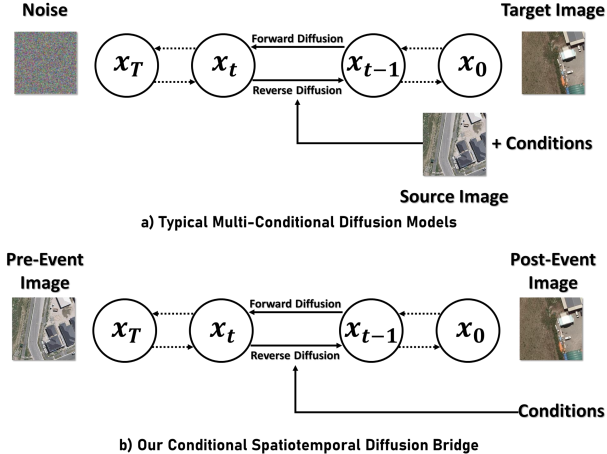


Figure 2. Comparison between (a) typical multi-conditional diffusion models and (b) our conditional spatiotemporal diffusion bridge. Instead of noise-to-image diffusion, ChangeBridge adapts a stochastic Brownian-bridge diffusion model with additional multimodal event controls, directly modeling the multi-conditional (pre-event images and multimodal event controls) spatiotemporal mapping.

ture scenarios based on past observations—i.e., modeling the spatiotemporal evolution of a given scene under multimodal conditions. Addressing this challenge could unlock valuable applications in fields such as urban planning, land management, and scenario forecasting.

In this work, we propose **ChangeBridge**, a multimodal-controlled spatiotemporal generative method for remote sensing. ChangeBridge generates post-event images from given pre-event images, allowing flexible multimodal event control signals (e.g., text prompts, instance layouts, or semantic maps). Fig. 1 shows some examples of ChangeBridge to synthesize realistic future scenes, conditioned on given pre-event images and multimodal event controls.

The multimodal cross-spatiotemporal generation capability of ChangeBridge originates from a tailored **Conditional Spatiotemporal Diffusion Bridge**. Instead of using typical diffusion models [12, 29, 30] that generate images from random noise, we adapt a stochastic Brownian-bridge diffusion [16] to model the conditional spatiotemporal generative process. This spatiotemporal mapping is multi-conditional that integrates both the pre-event image and multimodal control signals.

The difference between our conditional spatiotemporal diffusion bridge and typical multi-conditional diffusion models is illustrated in Fig. 2. This bridge formulation guarantees a direct cross-temporal trajectory under multimodal event controls in the latent space. These multimodal event controls—such as text prompts, instance layouts, and semantic maps—are dynamically injected into the denoising process via cross-attention mechanism.

Experiments on quantitative and qualitative evaluations

demonstrate that ChangeBridge generates high-fidelity post-event images, while ensuring the generative alignment with given pre-event images and multimodal control signals. Further evaluations through the downstream change detection tasks, demonstrate the semantic consistency of our generated images. With realistic spatiotemporal change generation, the synthesized data from ChangeBridge further proves to significantly augment the accuracy of change detection, achieving a 3.11% IoU increase on the WHU-CD dataset.

Our contributions can be summarized as follows:

- We propose ChangeBridge, a cross-spatiotemporal generative model, synthesizing post-event images based on given pre-event imagery and multimodal control signals.
- We design a conditional spatiotemporal diffusion bridge, directly modeling structured and controllable spatiotemporal generation trajectories.
- ChangeBridge supports future scenario simulation in remote sensing, and can serve as a generative data augmentation tool for change detection tasks.

## 2. Related work

### 2.1. Multi-Conditional Diffusion Generation

Multi-condition diffusion models are widely used to incorporate multiple control signals as inputs to guide controllable generation. For example, LDM [23] combines multiple conditions using concatenation or cross-attention. UNIT-DDPM [27] combines two diffusion models with domain translation. ControlNet [45] integrates spatial control via attention mechanisms in large pre-trained models, enabling fine-grained modifications. GLIGEN [18] incorporates additional layouts, images, or other conditions into the text-to-image diffusion model. DreamBooth [25] fine-tunes a pre-trained diffusion model to personalize generation, embedding specific subjects or styles into diffusion models.

Although these pioneering works have successfully implemented multi-condition control, they are all based on a noise-to-image architecture. Therefore, they must adopt complex methods to ensure the alignment of multiple conditions, such as guidance-free techniques [9], LoRA [38], or projected sampling [40].

Some diffusion bridge-based works [16, 49], such as BBDM [16], have emerged, establishing image-to-image diffusion processes that facilitate smoother transitions between images. In this work, inspired by these advancements, we establish a conditional spatiotemporal diffusion bridge, incorporating multimodal control mechanism, which guarantees a more stable and coherent cross-spatiotemporal transition under multimodal controls.

## 2.2. Spatiotemporal Scenario Simulation

Spatiotemporal scenario simulation plays a crucial role in understanding land use changes and urban dynamics. Traditional methods in this area primarily rely on rule-based algorithms [4, 8, 24], statistical models [22, 33] and game engine [3] to generate land use scenarios. While effective for basic spatial analysis, these approaches fail to realistically simulate environmental changes.

More recently, generative models have brought new vitality to spatiotemporal scenario simulation. Changen [47] uses GANs to generate post-event scenes by modifying conditioned change maps, while Changen2 [48] incorporates a diffusion model for scalable spatiotemporal scenario generation. ChangeAnywhere [32] utilizes an unconditional diffusion model and XOR operations to generate pre-event and post-event images. ChangeDiff [42] combines text-to-layout and layout-to-image modules to generate spatiotemporal scenario based on text prompts.

These excellent change generation methods typically modify conditions to model spatial changes but fail to generate changes based on given pre-event images. In contrast, we propose ChangeBridge, which models temporal generation under multimodal spatial controls while aligning with the given pre-event images.

## 3. Preliminary

We first introduce the latent diffusion model (LDM), which applies diffusion in a low-dimensional latent space, reducing computational cost [23]. It consists of: a) an autoencoder, b) a forward diffusion process, c) a reverse inference process, d) a training objective, and e) an autoencoder. Given an image  $\mathbf{x}_0$ , the pre-trained autoencoder  $\mathcal{E}$  encodes it into a latent representation  $\mathbf{z}_0 = \mathcal{E}(\mathbf{x}_0)$ , where the latent distribution denotes as  $\mathbf{z}_0 \sim q(\mathbf{z}_0)$ .

**Forward process.** The Gaussian noise  $\epsilon \sim \mathcal{N}(\mathbf{0}, \mathbf{I})$  is added over  $T$  timesteps with a predefined schedule  $\{\alpha_t\}_{t=0}^T$ , yielding noisy latents  $\mathbf{z}_T$ . The noise update rule follows  $\mathbf{z}_t = \sqrt{\alpha_t}\mathbf{z}_0 + \sqrt{1 - \alpha_t}\epsilon$ , and then forms a Markov chain  $q(\mathbf{z}_1, \dots, \mathbf{z}_T | \mathbf{z}_0) = \prod_{t=1}^T q(\mathbf{z}_t | \mathbf{z}_{t-1})$ . The forward transition distribution is  $q(\mathbf{z}_t | \mathbf{z}_{t-1}) = \mathcal{N}(\mathbf{z}_t; \mu(\mathbf{z}_{t-1}, t), \sigma^2(t)\mathbf{I})$ , with the mean  $\mu(\mathbf{z}_{t-1}, t) = \sqrt{1 - \alpha_t}\mathbf{z}_{t-1}$  and the variance  $\sigma^2(t) = \alpha_t$ .

**Reverse process.** The original latent  $\mathbf{z}_0$  is reconstructed from  $\mathbf{z}_T$  using a denoising network  $\epsilon_\theta$ , modeled with the reverse transition distribution  $p_\theta(\mathbf{z}_{t-1} | \mathbf{z}_t) = \mathcal{N}(\mathbf{z}_{t-1}; \hat{\mu}_\theta(\mathbf{z}_t, t), \hat{\sigma}_\theta^2(t)\mathbf{I})$ . Here,  $\hat{\mu}_\theta(\mathbf{z}_t, t)$  and  $\hat{\sigma}_\theta^2(t)$  are the estimated mean and variance by the denoising network  $\epsilon_\theta$ .

**Training objective.** The denoising network  $\epsilon_\theta$  is optimized to predict the added noise via

$$\mathcal{L} = \mathbb{E}_{t, \mathbf{x}_0, \epsilon \sim \mathcal{N}(0, \mathbf{I})} [\|\epsilon - \hat{\epsilon}_\theta(\mathbf{z}_t, t)\|_2^2]. \quad (1)$$

The pre-trained autoencoder  $\mathcal{D}$  reconstructs the final image  $\mathbf{x}'_0 = \mathcal{D}(\mathbf{z}'_0)$ .

This pipeline shows the typical noise-to-image diffusion generation scheme, starting from the image  $\mathbf{z}_0 \sim q(\mathbf{z}_0)$ , evolving to the noise  $\mathbf{z}_T \sim \mathcal{N}(0, \mathbf{I})$ . And training the model to reverse the process via the training objective  $\mathcal{L}$ .

## 4. Methodology

### 4.1. Problem Definition

The noise-to-image diffusion framework is theoretically incapable of providing a direct generative mapping between the pre-event and post-event domains. Therefore, to enable effective cross-spatiotemporal generation, it is necessary to tailor a diffusion process that explicitly models the transition between pre-event and post-event scenarios. Instead of treating the generation as an unconditional sampling process from a random noisy distribution, we need to establish a structured spatiotemporal diffusion bridge that connects the latent representations of the two domains.

Formally, let  $\mathbf{x}_a$  and  $\mathbf{x}_b$  denote two remote-sensing images sampled from the pre-event and post-event domains, respectively. To keep the computational cost low, we conduct the diffusion process in the latent space following LDM [23]. The corresponding latent representations are obtained through an autoencoder  $\mathcal{E}$ , such that  $\mathbf{z}_a = \mathcal{E}(\mathbf{x}_a)$  and  $\mathbf{z}_b = \mathcal{E}(\mathbf{x}_b)$ , where  $\mathbf{z}_a, \mathbf{z}_b \in \mathbb{R}^{n \times m}$  and  $n \times m$  denotes the latent space dimension. We assume that the pre-event distribution follows  $\mathbf{z}_a \sim q_{\text{pre}}(\mathbf{z}_a)$  and the post-event distribution follows  $\mathbf{z}_b \sim q_{\text{post}}(\mathbf{z}_b)$ , both approximated as standard Gaussian distributions  $\mathcal{N}(\mathbf{0}, \mathbf{I})$ .

Additionally, we introduce a conditional input  $\mathbf{x}_c$ , representing auxiliary multimodal guidance such as instance layouts, semantic maps, or text prompts. The condition is encoded into a latent representation  $\mathbf{z}_c = \tau_\theta(\mathbf{x}_c)$ , where  $\tau_\theta$  is a domain-specific conditional encoder mapping  $\mathbf{x}_c$  into  $m \times n$ . The objective is to learn a generative mapping from  $(\mathbf{z}_a, \mathbf{z}_c)$  to a plausible post-event latent  $\mathbf{z}'_b$ , ensuring that the reconstructed image  $\mathbf{x}'_b = \mathcal{D}(\mathbf{z}'_b)$  accurately reflects event-driven changes while preserving semantic consistency with  $\mathbf{x}_a$ .

### 4.2. Conditional Spatiotemporal Diffusion Bridge

Inspired by BBDM [16], we introduce a stochastic Brownian bridge process [20, 35]. It is a continuous-time stochastic model that satisfies the Markov, Gaussian, and stationarity properties, and can evolve from a fixed starting state to a fixed ending state. Specifically, the state distribution at each timestep  $t$  in a diffusion bridge, starting at the initial point  $\mathbf{z}_0 \sim q(\mathbf{z}_0)$  at time  $t = 0$  and ending at the final point  $\mathbf{z}_T$  at

time  $t = T$ , is expressed as:

$$p(\mathbf{z}_t | \mathbf{z}_0, \mathbf{z}_T) = \mathcal{N} \left( \left(1 - \frac{t}{T}\right) \mathbf{z}_0 + \frac{t}{T} \mathbf{z}_T, \frac{t(T-t)}{T} \mathbf{I} \right). \quad (2)$$

Based on the stochastic Brownian bridge process, we model the controllable spatiotemporal diffusion process, called ChangeBridge, for cross-spatiotemporal generation with multimodal controls. The diffusion process of ChangeBridge can be guided by multiple conditions, as presented in Fig. 2.

In the following sections, ChangeBridge is primarily described in four parts: a) Forward process in Sec. 4.2.1. b) Reverse process in Sec. 4.2.2. c) Training objective in Sec. 4.2.3. d) Conditioned guidance in Sec. 4.2.4.

#### 4.2.1. Forward Process.

The forward process is a noise-adding process, ensuring that after  $T$  time steps, the transition can be reached from the post-event latent  $\mathbf{z}_b$  to the pre-event latent  $\mathbf{z}_a$ . For each timestep  $t$ , we need to compute the variance  $\sigma^2(t)$  and mean  $\mu$  of the Gaussian-distributed noise.

Specifically, this forward process starts from the post-event latent  $\mathbf{z}_b$  (i.e.,  $\mathbf{z}_0 = \mathbf{z}_b$ ) and ending with the pre-event latent  $\mathbf{z}_a$  (i.e.,  $\mathbf{z}_T = \mathbf{z}_a$ ), where the probability distribution is  $(\mathbf{z}_0, \mathbf{z}_T) \sim q(\mathbf{z}_b, \mathbf{z}_a)$ . We denote the  $t$ -th intermediate state of the post-event latent as  $\mathbf{z}_t$ . The new marginal distribution  $q(\mathbf{z}_t | \mathbf{z}_0, \mathbf{z}_T)$ , according to the definition of the stochastic Brownian bridge process in Eq. (2), can be derived as:

$$q(\mathbf{z}_t | \mathbf{z}_0, \mathbf{z}_T) = q(\mathbf{z}_t | \mathbf{z}_b, \mathbf{z}_a) = \mathcal{N}(\mathbf{z}_t; (1 - m_t)\mathbf{z}_b + m_t\mathbf{z}_a, \delta_t \mathbf{I}), \quad (3)$$

where  $m_t = \frac{t}{T}$  and the variance term  $\delta_t = 2(m_t - m_t^2)$  represent the spread of the intermediate state  $\mathbf{z}_t$ . Then, the intermediate state of the post-event latent  $\mathbf{z}_t$  can be computed in discrete form as follows:

$$\begin{aligned} \mathbf{z}_t &= (1 - m_t)\mathbf{z}_b + m_t\mathbf{z}_a + \sqrt{\delta_t} \boldsymbol{\epsilon}, \\ \mathbf{z}_{t-1} &= (1 - m_{t-1})\mathbf{z}_b + m_{t-1}\mathbf{z}_a + \sqrt{\delta_{t-1}} \boldsymbol{\epsilon}, \end{aligned} \quad (4)$$

where  $\boldsymbol{\epsilon} \sim \mathcal{N}(\mathbf{0}, \mathbf{I})$  is Gaussian noise sampled from the unit covariance matrix. Consequently, the forward transition distribution  $q(\mathbf{z}_t | \mathbf{z}_{t-1}, \mathbf{z}_a)$  in the spatiotemporal diffusion bridge can be derived from Eq. (4) as follows:

$$q(\mathbf{z}_t | \mathbf{z}_{t-1}, \mathbf{z}_a) = \mathcal{N}(\mathbf{z}_t; \mu(\mathbf{z}_{t-1}, t, \mathbf{z}_a), \sigma^2(t) \mathbf{I}). \quad (5)$$

The post-event latent variable  $\mathbf{z}_t$  follows a Gaussian distribution. Here, the mean is  $\mu(\mathbf{z}_{t-1}, t, \mathbf{z}_a) = \frac{1-m_t}{1-m_{t-1}} \mathbf{z}_{t-1} + \left(m_t - \frac{1-m_t}{1-m_{t-1}} m_{t-1}\right) \mathbf{z}_a$ . The variance is given by  $\sigma^2(t) = \delta_{t|t-1}$ , and we can express this variance as  $\delta_{t|t-1} = \delta_t - \delta_{t-1} \frac{(1-m_{t-1})^2}{(1-m_t)^2}$ . When the diffusion process reaches the

final timestep  $t = T$ , we have  $m_T = 1$  and consequently  $\mathbf{z}_T = \mathbf{z}_a$ . The forward process thus defines a precise noise-adding transition from post-event state  $\mathbf{z}_b$  to pre-event state  $\mathbf{z}_a$ .

#### 4.2.2. Reverse Process

The reverse process of our spatiotemporal diffusion bridge begins from the pre-event latent  $\mathbf{z}_a$  (i.e.,  $\mathbf{z}_T = \mathbf{z}_a$ ) instead of Gaussian noise. This process aims to reconstruct the post-event latent  $\mathbf{z}_b$  (i.e.,  $\mathbf{z}_0 = \mathbf{z}_b$ ) through a denoising network  $\epsilon_\theta$ . This denoising network  $\epsilon_\theta$  iteratively recovers the next post-event latent  $\mathbf{z}_{t-1}$ , given the current post-event latent  $\mathbf{z}_t$  and the original pre-event latent  $\mathbf{z}_a$ . Also, the Brownian-bridge reverse process can be modeled as a Markov chain, and the reverse transition distribution  $p_\theta(\mathbf{z}_{t-1} | \mathbf{z}_t, \mathbf{z}_a)$  can be defined as a Gaussian distribution:

$$p_\theta(\mathbf{z}_{t-1} | \mathbf{z}_t, \mathbf{z}_a) = \mathcal{N}(\mathbf{z}_{t-1}; \hat{\boldsymbol{\mu}}_\theta(\mathbf{z}_t, t, \mathbf{z}_a), \hat{\sigma}_\theta^2(t) \mathbf{I}), \quad (6)$$

where  $\hat{\boldsymbol{\mu}}_\theta(\mathbf{z}_t, t, \mathbf{z}_a)$  is the estimated mean and  $\hat{\sigma}_\theta^2(t)$  is the variance.

#### 4.2.3. Training Objective

In the Brownian-bridge spatiotemporal diffusion model, training involves optimizing the evidence lower bound (ELBO), which is given by the following equation:

$$\begin{aligned} \mathcal{L} &= -\mathbb{E}_q \left[ \sum_{t=2}^T D_{KL}(q(\mathbf{z}_{t-1} | \mathbf{z}_t, \mathbf{z}_0, \mathbf{z}_a) \right. \\ &\quad \left. || p_\theta(\mathbf{z}_{t-1} | \mathbf{z}_t, \mathbf{z}_a) - \log p_\theta(\mathbf{z}_0 | \mathbf{z}_1, \mathbf{z}_a) \right]. \end{aligned}$$

The terms  $p_\theta(\mathbf{z}_{t-1} | \mathbf{z}_t, \mathbf{z}_a)$  and  $\log p_\theta(\mathbf{z}_0 | \mathbf{z}_1, \mathbf{z}_a)$  can be obtained using Eq. (6). In this setup, the pre-event latent  $\mathbf{z}_a$  is fixed, so the last term becomes a constant and can be ignored. We then can apply Bayes' theorem and the Markov chain property to derive  $q(\mathbf{z}_{t-1} | \mathbf{z}_t, \mathbf{z}_0, \mathbf{z}_a)$  as:

$$q(\mathbf{z}_{t-1} | \mathbf{z}_t, \mathbf{z}_0, \mathbf{z}_a) = \mathcal{N} \left( \mathbf{z}_{t-1}; \hat{\boldsymbol{\mu}}_t(\mathbf{z}_t, \mathbf{z}_0, \mathbf{z}_a), \tilde{\delta}_t \mathbf{I} \right). \quad (7)$$

Here, the mean  $\hat{\boldsymbol{\mu}}_t$  is given by:

$$\hat{\boldsymbol{\mu}}_t(\mathbf{z}_t, \mathbf{z}_0, \mathbf{z}_a) = c_{bt} \mathbf{z}_t + c_{at} \mathbf{z}_a + c_{et} \mathbf{z}_0, \quad (8)$$

where the coefficients are defined as  $c_{bt} = \frac{\delta_{t-1}}{\delta_t} \frac{1-m_t}{1-m_{t-1}} + \frac{\delta_{t|t-1}}{\delta_t} (1 - m_{t-1})$ ,  $c_{at} = m_{t-1} - m_t \frac{1-m_t}{1-m_{t-1}} \frac{\delta_{t-1}}{\delta_t}$ , and  $c_{et} = (1 - m_{t-1}) \frac{\delta_{t|t-1}}{\delta_t}$ . The variance  $\tilde{\delta}_t$  is computed as  $\frac{\delta_{t|t-1} \cdot \delta_{t-1}}{\delta_t}$ .

Considering  $\mathbf{z}_0$  is unknown during inference, we use a reparameterization approach similar to that in DDPM. The key idea is to replace  $\mathbf{z}_b$  with a noise variable  $\boldsymbol{\epsilon}$  in the mean term. With the denoising network  $\theta$  estimating the added noise  $\boldsymbol{\epsilon}_\theta$ , the mean  $\hat{\boldsymbol{\mu}}_\theta$  is represented as:

$$\hat{\boldsymbol{\mu}}_\theta(\mathbf{z}_t, \mathbf{z}_a, t) = c_{bt} \mathbf{z}_t + c_{at} \mathbf{z}_a + c_{et} \boldsymbol{\epsilon}_\theta(\mathbf{z}_t, t, \mathbf{z}_a). \quad (9)$$

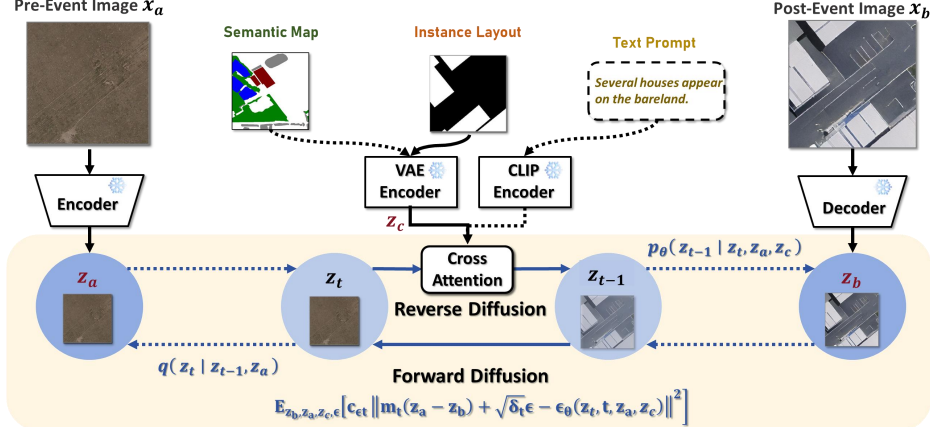


Figure 3. Framework of ChangeBridge, which construct a conditional spatiotemporal diffusion bridge process for cross-spatiotemporal generation with multimodal. Given the pre-event images  $x_a$  and multimodal controls  $x_c$  (e.g., text prompts, semantic maps, instance layouts), ChangeBridge can generate post-event images  $x_b$ , synthesizing both event and event-driven background variations.

Thus, the training objective for our spatiotemporal diffusion bridge in Eq. (7) can be simplified to:

$$\mathcal{L} = \mathbb{E}_{z_b, z_a, \epsilon} \left[ c_{\epsilon t} \|m_t(z_a - z_b) + \sqrt{\delta_t} \epsilon - \epsilon_\theta(z_t, t, z_a)\|^2 \right], \quad (10)$$

where  $z_b$  is the initial state  $z_0$ , and  $c_{\epsilon t}$  is a weighting factor, typically set to  $\frac{1}{t}$ , and  $\delta_t$  is a fixed variance schedule defined by  $\delta_t = 2(m_t - m_t^2)$ .

The inference process employs the deterministic ordinary differential equation (ODE) sampling, similar to DDPM [12]. Given an inference timesteps  $\{t'_s\}_{s=1}^S \in \{1, 2, \dots, T\}$ , the conditional sampling process is formulated as:

$$z_{t'_{s-1}} = c_{bt'_s} z_t + c_{at'_s} z_a - c_{\epsilon t'_s} \epsilon_\theta(z_{t'_s}, t'_s, z_a) + \sqrt{\delta_{t'_s}} \epsilon \quad (11)$$

Unlike typical diffusion models, the training objective of our ChangeBridge is anchored at the pre-event state  $z_a$  and the post-event state  $z_b$ , establishing a strict diffusion trajectory for cross-spatiotemporal change generation.

#### 4.2.4. Conditional Guidance

Existing diffusion models [13, 44] have demonstrated their capability of modeling the conditional distribution  $x_c$ . Following Stable Diffusion [30], we adopt the cross-attention mechanism  $\text{Attn}(Q, K, V)$ , incorporating domain-specific conditional latent  $z_c = \tau_\theta(x_c)$  to enable multimodal control for the ChangeBridge’s change generation.

Specifically, we introduce the domain-specific conditional encoder  $\tau_\theta$  that projects  $x_c$  to an intermediate latent representation  $z_c = \tau_\theta(x_c) \in \mathbb{R}^{M \times d_\tau}$ . Then,  $z_c$  is mapped to the intermediate layers of the denoising network  $\epsilon_\theta$  via a cross-attention layer implementing

$$\text{Attn}(Q, K, V) = \text{softmax} \left( \frac{QK^T}{\sqrt{d}} \right) \cdot V, \quad (12)$$

Here,  $\varphi_i(z_t) \in \mathbb{R}^{N \times d_i}$  denotes a flattened intermediate latent representation of denoising network  $\epsilon_\theta$ . We use the intermediate latent of the denoising network  $\varphi_i(z_t)$  as the query  $Q = W_Q^{(i)} \cdot \varphi_i(z_t)$ . The conditional intermediate latent  $z_c$  served as the key  $K = W_K^{(i)} \cdot \tau_\theta(x_c)$  and the value  $V = W_V^{(i)} \cdot \tau_\theta(x_c)$ . And  $W_V^{(i)} \in \mathbb{R}^{d \times d_i}$ ,  $W_Q^{(i)} \in \mathbb{R}^{d \times d_\tau}$ ,  $W_K^{(i)} \in \mathbb{R}^{d \times d_\tau}$  are learnable projection matrices [34].

Based on multimodal controls (e.g. text prompts, instance layouts, semantic maps), we learn the conditional spatiotemporal diffusion bridge via

$$\mathcal{L}_{\text{cond}} = \mathbb{E}_{z_b, z_a, z_c, \epsilon} \left[ c_{\epsilon t} \|m_t(z_a - z_b) + \sqrt{\delta_t} \epsilon - \epsilon_\theta(z_t, t, z_a, z_c)\|^2 \right]. \quad (13)$$

Finally, we obtain the generative post-event image  $x'_b$  from the reconstruction of the pre-trained autoencoder  $\mathcal{D}(z'_b)$ , based on given pre-event images  $x_a$  and multimodal control  $x_c$ .

## 5. Experiments

### 5.1. Experimental Setting

**Dataset descriptions.** We conduct experiments on four widely used change detection datasets: 1) LEVIR-CC [6], used for conditioning on text prompts; 2) WHU-CD [14] and S2Looking [28], used for conditioning on instance layouts; and 3) SECOND [37], used for conditioning on semantic maps. For the change detection task, we evaluate the synthesized data as aggregation on WHU-CD and S2Looking.

**Implementation details.** We train the Brownian bridge denoising network from scratch for 3,000 epochs using  $256 \times 256$  images, which are downsampled to a  $64 \times 64$  latent space via a pre-trained VQGAN [23] with a down-sampling factor of  $f = 4$ . The training process employs a batch size of 16, pairing pre-event images with change masks. The number of Brownian bridge time steps are set to 1,000 during training and 200 during inference. The network optimization is performed using AdamW with a learning rate of  $1.0 \times 10^{-5}$  and a decay rate of  $\gamma = 0.2$ . For latent extraction of the instance layouts and semantic maps, we adopt the same pre-trained VQGAN [10] model as used in the Latent Diffusion Model [23]. For latent extraction of the text prompts, we use CLIP [21] with the ViT-B/32 variant.

## 5.2. Comparison with Multi-Conditional Methods

To evaluate the effectiveness of our ChangeBridge, we compare it with existing multi-conditional generative methods. The comparison includes four image editing approaches categorized based on their control modalities. For image-controlled generation, we consider UNITE [43] and ControlNet [44], both of which incorporate IP-Adapter (IPA) [39] to condition the generation process on instance layouts and semantic maps. For text-controlled generation, we include DreamBooth [25] and ELITE [36], which rely on textual prompts to guide the synthesis. This comparison allows us to assess the effectiveness of ChangeBridge across different conditioning modalities, demonstrating its advantages in handling structured spatial controls in a cross-temporal diffusion bridge process.

**Qualitative results.** We present qualitative comparisons of ChangeBridge against existing multi-conditional generative methods. The results for instance layouts, semantic maps, and text prompts conditioning are shown in Fig. 4, Fig. 5, and Fig. 6, respectively.

For instance layout-based generation, ChangeBridge effectively aligns with the given spatial constraints while preserving realistic textures and structural consistency. Compared to UNITE and ControlNet+IPA, our approach produces clearer structures with more natural object placements. The generated buildings align well with the predefined layouts, demonstrating the model’s ability to adhere to structural priors while maintaining high visual fidelity.

For semantic map-based generation, ChangeBridge surpasses other methods in generating semantically accurate and visually coherent results. The generated images exhibit better structural alignment with the given semantic map, as well as sharper and more diverse textures. As highlighted by the red boxes in Fig. 5, ChangeBridge successfully maintains consistency in building regions while mitigating artifacts present in UNITE and ControlNet+IPA generations.

For text prompt-based generation, ChangeBridge excels in translating textual descriptions into realistic satellite imagery. It effectively synthesizes features such as roads and residential areas with high semantic consistency. Compared to DreamBooth and ELITE, ChangeBridge generates clearer and more contextually appropriate structures. The synthesized samples show improved alignment with the described scene, such as the structured arrangement of houses and the accurate positioning of roads in forested regions.

Overall, ChangeBridge consistently outperforms existing image-editing methods across all conditioning modalities, achieving superior visual quality, semantic consistency, and structural alignment.

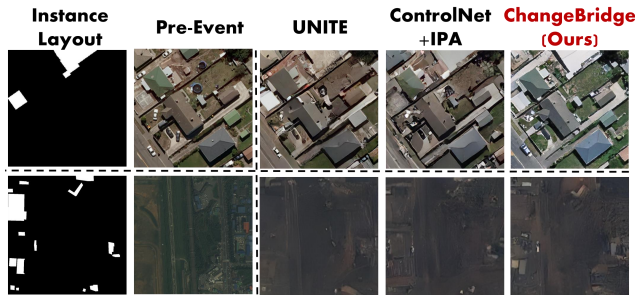


Figure 4. Comparison to methods conditioned on **instance layouts**. These methods of image editing include UNITE, and ControlNet incorporating IP-Adapter (IPA).



Figure 5. Comparison to methods conditioned on **semantic maps**. These methods of image editing include UNITE, and ControlNet incorporating IP-Adapter (IPA). The red boxes illustrate the misalignments between the generated content and the intended semantic maps.

**Quantitative results.** We report the quantitative evaluation results using Fréchet Inception Distance (FID) [11] and Inception Score (IS) [26] on four datasets, as shown in Tab. 1. Lower FID values indicate better perceptual quality and diversity, while higher IS values suggest improved realism and semantic meaningfulness of the generated images. As suggested, we additionally evaluate alignment using a segmentation model (SegFormer) for the semantic-map and instance-layout conditions, and CLIP-based Cosine similarity scores for the text-prompt condition (see Tab. 1). The

Table 1. Comparison of synthesized sample quality under instance layout, semantic map, and text prompt conditioning. FID and IS are reported for all settings; mIoU for semantic maps, IoU for instance layouts, and cosine similarity (CosSim) for text prompts. Real data results serve as the upper bound. ControlNet\* denotes ControlNet combined with IP-Adapter (ControlNet+IPA).

Semantics	SECOND			Layouts	WHU-CD		S2Looking			Texts	LEVIR-CC			
	FID ↓	IS ↑	mIoU ↑		FID ↓	IS ↑	IoU ↑	FID ↓	IS ↑		IoU ↑	FID ↓	IS ↑	CosSim ↑
Real Data	-	-	76.19	Real Data	-	-	81.30	-	-	82.47	Real Data	-	-	0.89
UNITE	96.81	5.76	70.22	UNITE	96.81	5.76	69.38	197.57	3.98	72.61	DreamBooth	275.64	1.52	0.78
ControlNet*	120.81	3.31	72.30	ControlNet*	52.08	5.12	74.54	94.68	4.56	75.20	ELITE	102.08	3.34	0.84
<b>Ours</b>	<b>98.42</b>	<b>5.57</b>	<b>73.46</b>	<b>Ours</b>	<b>39.23</b>	<b>6.35</b>	<b>77.96</b>	<b>59.25</b>	<b>4.62</b>	<b>79.33</b>	<b>Ours</b>	<b>67.23</b>	<b>4.63</b>	<b>0.86</b>



Figure 6. Comparison to methods conditioned on **text prompts**. These methods of image editing include DreamBooth and ELITE.

first row shows results of real data, serving as the upper bound.

For semantic map-conditioned generation, ChangeBridge outperforms existing methods on the SECOND dataset, achieving the lowest FID of 98.42 and the highest IS of 5.57. Compared to UNITE and ControlNet+IPA, which yield FID scores of 162.70 and 120.81 respectively, ChangeBridge significantly enhances image quality while maintaining high semantic consistency.

For instance layout-conditioned generation, we evaluate performance on the WHU-CD and S2Looking datasets. On WHU-CD, ChangeBridge achieves a FID of 39.23 and an IS of 6.35, surpassing UNITE by 57.58 in FID and ControlNet+IPA by 12.85. Similarly, on S2Looking, ChangeBridge achieves a FID of 59.25, significantly outperforming UNITE (197.57) and ControlNet+IPA (94.68). The higher IS scores further demonstrate that ChangeBridge produces more diverse and realistic samples.

For text prompt-conditioned generation, ChangeBridge achieves strong performance on LEVIR-CC, reducing the FID to 67.23 while increasing IS to 4.63. In contrast, DreamBooth and ELITE obtain FID scores of 275.64 and 102.08 respectively, with IS values remaining relatively low. This highlights the effectiveness of ChangeBridge in capturing text-guided semantic attributes while maintaining fidelity and diversity.

Across all conditioning modalities, ChangeBridge consistently achieves the lowest FID and highest IS, demonstrating its effectiveness in multimodal cross-

spatiotemporal image synthesis.

### 5.3. Evaluation on Downstream Change Detection

In this section, we further evaluate the effectiveness of ChangeBridge by applying its synthesized data as augmentation on downstream change detection tasks. Specifically, we use the OpenCD toolkit [17] with four baselines: BiT [7], STANet [6], ChangeFormer [2], and ChangeStar [46]. Evaluation metrics include F1 score and IoU. More detailed descriptions of datasets and implementations can be found in the appendix.

#### 5.3.1. Augmentation Scale

We experiment with various ratios  $R \in \mathbb{N}$  of original to synthetic data  $\mathcal{B}$ , where  $|\mathcal{B}'| = R \cdot |\mathcal{B}|$ . We quantify training performance in joint data  $\mathcal{B} \cup \mathcal{B}'$  versus original data  $\mathcal{B}$ . Table 2 shows that the incorporation of synthetic data improves the performance of both datasets. For the WHU-CD dataset, optimal results occur at  $R = 2$ , with the F1 score increasing from 83.98% to 86.27% and IoU from 72.39% to 74.65%. On the S2Looking dataset, peak performance is at  $R = 1$ , achieving an F1-score of 64.05% and IoU of 48.11%, with improvements of +1.69%. Conclusively, The training set combines original data ( $\mathcal{B}$ ) and synthetic data ( $\mathcal{B}'$ ) in a 1:1 ratio to perform the best results on the WHU-CD dataset, and that of 1:2 on the S2Looking dataset.

Table 2. Augmentation scale with different mixing ratios of the original data  $\mathcal{B}$  and synthetic data  $\mathcal{B}'$  for training change detection. F1 score (%) and IoU (%) are reported with the BiT baseline.

Data	WHU-CD		S2Looking	
	F1 ↑	IoU ↑	F1 ↑	IoU ↑
$\mathcal{B}$	83.98	72.39	62.74	46.94
$\mathcal{B} \cup \mathcal{B}'$	85.06	73.21	<b>64.05</b>	<b>48.11</b>
$\mathcal{B} \cup 2\mathcal{B}'$	<b>86.27</b>	<b>74.65</b>	63.96	48.03
$\mathcal{B} \cup 3\mathcal{B}'$	84.98	73.40	63.22	47.45

#### 5.3.2. Performance Improvements

Table 3 shows the improvements of our methods across all baselines. Our ChangeBridge consistently enhances change detection performance across different models and datasets.

On the WHU-CD dataset, ChangeBridge improves the F1-score of STANet, BiT, ChangeStar, and ChangeFormer by +1.52%, +2.29%, +2.88%, and +2.38%, respectively, while the IoU gains range from +2.12% to +3.11%. Similarly, on the S2Looking dataset, ChangeBridge leads to F1-score increases of up to +2.27% and IoU improvements of up to +1.70%. Notably, ChangeFormer achieves the highest performance boost among all baselines, highlighting the adaptability of our augmentation to transformer-based architectures. These results confirm that ChangeBridge provides a strong data augmentation strategy, significantly benefiting change detection models by improving their ability to capture and recognize meaningful scene transformations.

Table 3. Improvement of the data augmentation of our ChangeBridge for downstream change detection models. F1 score (%) and IoU (%) are reported.

Method	WHU-CD		S2Looking	
	F1 ↑	IoU ↑	F1 ↑	IoU ↑
STANet	69.37	53.11	57.22	40.81
<b>+Ours</b>	<b>70.89</b> <sup>+1.52</sup>	<b>55.42</b> <sup>+2.31</sup>	<b>58.14</b> <sup>+0.92</sup>	<b>42.30</b> <sup>+1.49</sup>
BiT	83.98	72.39	62.74	46.94
<b>+Ours</b>	<b>86.27</b> <sup>+2.29</sup>	<b>74.65</b> <sup>+2.26</sup>	<b>64.05</b> <sup>+1.31</sup>	<b>48.11</b> <sup>+1.17</sup>
ChangeStar	84.16	74.02	66.30	49.75
<b>+Ours</b>	<b>87.04</b> <sup>+2.88</sup>	<b>77.13</b> <sup>+3.11</sup>	<b>68.57</b> <sup>+2.27</sup>	<b>51.36</b> <sup>+1.61</sup>
ChangeFormer	85.05	74.92	65.76	48.99
<b>+Ours</b>	<b>87.43</b> <sup>+2.38</sup>	<b>77.04</b> <sup>+2.12</sup>	<b>68.01</b> <sup>+2.25</sup>	<b>50.69</b> <sup>+1.70</sup>

### 5.3.3. Comparison with Change Synthesis Methods

We evaluate ChangeBridge against existing change synthesis methods under two different training settings: adaptation learning and zero-shot learning. In both cases, the models are evaluated on real test data, but the way synthetic and real data are utilized in training differs. Adaptation learning involves pre-training on synthetic data and then fine-tuning on real-world data, measuring how well the synthetic-to-real transfer enhances change detection. In contrast, zero-shot learning relies solely on synthetic data for training, with models tested directly on real data without any fine-tuning.

**Adaptation performance.** Table 4 presents the adaptation performance on the S2Looking dataset, where models undergo pre-training on synthetic data before being fine-tuned on real-world images. The results show that ChangeBridge consistently outperforms all competing methods, particularly those that do not leverage pre-event images.

The overall performance of change synthesis methods incorporating pre-event images surpasses that of methods without pre-event guidance. The primary reason lies in the fact that a major challenge in change detection is background variation caused by cross-temporal factors, such as lighting changes, seasonal shifts, and human activities.

These factors introduce significant noise, making it difficult to isolate true structural changes.

Capturing such cross-temporal variations requires conditioning on pre-event images, which enables models to generate more realistic change representations. When pre-event images are incorporated, all methods demonstrate notable improvements, as they can explicitly account for these spatiotemporal variations rather than relying solely on inferred or heuristic-based change modeling.

Among pre-event-based approaches, ChangeBridge achieves the highest adaptation performance, improving the F1-score by +2.74 over the baseline, surpassing UNITE and ControlNet-IPA. This significant gain highlights the effectiveness of ChangeBridge’s spatiotemporal diffusion-based approach, which ensures better alignment with spatial structures and more semantically consistent change synthesis, ultimately leading to enhanced adaptation performance in real-world change detection tasks.

**Zero-shot performance.** To further assess generalization capability, we conduct a zero-shot evaluation on the WHU-CD dataset, with results presented in Table 5. Unlike the adaptation setting, where real data is introduced during training, zero-shot learning strictly relies on synthetic data. Despite this challenge, ChangeBridge achieves the highest performance, surpassing all other methods.

When pre-event images are incorporated, all methods demonstrate notable improvements. ChangeBridge outperforms both ControlNet-IPA and UNITE, achieving an F1-score of 79.25, which represents a +0.33 increase over ControlNet-IPA and +1.11 over UNITE. This improvement highlights the effectiveness of our spatiotemporal diffusion-based approach in synthesizing semantically consistent and spatially accurate changes, leading to enhanced generalization in real-world scenarios.

These findings reinforce the importance of pre-event-aware synthesis for both adaptation and zero-shot learning, demonstrating that ChangeBridge not only surpasses existing pre-event-based methods but also establishes a new benchmark for zero-shot change detection performance. The ability to align synthesized changes with spatiotemporal structures ensures that models trained solely on synthetic data can still yield highly reliable predictions in real-world environments.

### 5.4. Visualization of Example Diversity

As shown in Fig. 7, the generated samples exhibit significant variations across different examples while still adhering to the structural constraints imposed by the conditioning modalities. The instance layout ensures spatial control over object placement, the text prompts guide scene attributes and distributions, and the semantic maps maintain category consistency. The variations across the synthesized exam-

Table 4. Comparison of adaptation performance for change detection with change synthesizing methods, with ChangeStar as the baseline on the S2Looking dataset. F1 score (%) is reported.

Method		Adaptation
Baseline		66.30
w/o Pre-Event Input	+Copy-Paste	66.70
	+Inpainting	66.30
	+Changen	67.10
	+Changen2	67.30
w/ Pre-Event Input	+UNITE	67.89
	+ControlNet-IPA	68.02
	<b>+Ours</b>	<b>69.04<sup>+2.74</sup></b>

Table 5. Comparison of zero-shot performance for change detection with change synthesizing methods, with ChangeStar as the baseline on the WHU-CD dataset. F1 score (%) is reported.

Method		Zero-Shot
w/o Pre-Event Input	+Copy-Paste	3.80
	+Inpainting	21.80
	+Changen	26.60
	+Changen2	76.30
w/ Pre-Event Input	+UNITE	78.14
	+ControlNet-IPA	78.92
	<b>+Ours</b>	<b>79.25</b>

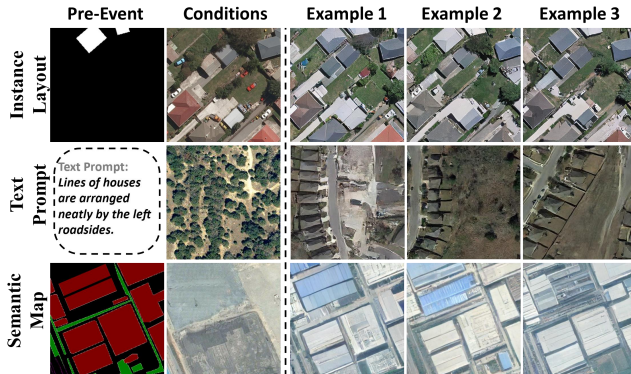


Figure 7. Example Diversity of our ChangeBridge, where sampling is performed under the same conditions and pre-event images.

ples confirm that our method effectively balances realism, control, and diversity. Furthermore, additional visualization results can be found in the Appendix.

## 6. Conclusion

In this work, we propose ChangeBridge, a cross-spatiotemporal generative model for remote sensing that incorporates multimodal spatial controls, including instance layouts, semantic maps, and text prompts. ChangeBridge

synthesizes post-event images from pre-event observations while maintaining fidelity and alignment through a spatiotemporal diffusion bridge, formulated as a stochastic Brownian bridge. Experimental results demonstrate its ability to generate high-quality future scenarios with realistic event-driven changes. Furthermore, ChangeBridge serves as an effective generative data augmentation technique, improving change detection performance.

## References

- [1] Orkhan Baghirli, Hamid Askarov, Imran Ibrahimli, Ismat Bakhishov, and Nabi Nabiyeu. Satdm: Synthesizing realistic satellite image with semantic layout conditioning using diffusion models. *arXiv preprint arXiv:2309.16812*, 2023. 1
- [2] Wele Gedara Chaminda Bandara and Vishal M Patel. A transformer-based siamese network for change detection. In *IGARSS 2022-2022 IEEE International Geoscience and Remote Sensing Symposium*, pages 207–210. IEEE, 2022. 7
- [3] N. Bourdis, D. Marraud, and H. Sahbi. Constrained optical flow for aerial image change detection. In *2011 IEEE International Geoscience and Remote Sensing Symposium*, pages 4176–4179. IEEE, 2011. 3
- [4] V Chaturvedi and WT de Vries. Machine learning algorithms for urban land use planning: A review. *Urban Science*, 5(3):68, 2021. 3
- [5] Bowen Chen, Liqin Liu, Chenyang Liu, Zhengxia Zou, and Zhenwei Shi. Spectral-cascaded diffusion model for remote sensing image spectral super-resolution. *IEEE Transactions on Geoscience and Remote Sensing*, 2024. 1
- [6] Hao Chen and Zhenwei Shi. A spatial-temporal attention-based method and a new dataset for remote sensing image change detection. *Remote Sensing*, 12(10):1662, 2020. 5, 7
- [7] Hao Chen, Zipeng Qi, and Zhenwei Shi. Remote sensing image change detection with transformers. *IEEE Transactions on Geoscience and Remote Sensing*, 60: 1–14, 2021. 7
- [8] A T Crooks, N W Gibin, and J J Heppenstall. A rule-based model of urban land use and economic growth. *International Journal of Geographical Information Science*, 24(2):311–331, 2010. 3
- [9] Prafulla Dhariwal and Alexander Nichol. Diffusion models beat gans on image synthesis. *Advances in neural information processing systems*, 34:8780–8794, 2021. 2
- [10] Patrick Esser, Robin Rombach, and Bjorn Ommer. Taming transformers for high-resolution image synthesis. In *Proceedings of the IEEE/CVF conference on computer vision and pattern recognition*, pages 12873–12883, 2021. 6

- [11] Martin Heusel, Hubert Ramsauer, Thomas Unterthiner, Bernhard Nessler, and Sepp Hochreiter. Gans trained by a two time-scale update rule converge to a local nash equilibrium. *Advances in neural information processing systems*, 30, 2017. 6
- [12] Jonathan Ho, Ajay Jain, and Pieter Abbeel. Denoising diffusion probabilistic models. In *NeurIPS*, 2020. 2, 5
- [13] Qihan Huang, Siming Fu, Jinlong Liu, Hao Jiang, Yipeng Yu, and Jie Song. Resolving multi-condition confusion for finetuning-free personalized image generation. *arXiv preprint arXiv:2409.17920*, 2024. 5
- [14] Shunping Ji, Shiqing Wei, and Meng Lu. Fully convolutional networks for multisource building extraction from an open aerial and satellite imagery data set. *IEEE Transactions on Geoscience and Remote Sensing*, 57(1):574–586, 2018. 5
- [15] Samar Khanna, Patrick Liu, Linqi Zhou, Chenlin Meng, Robin Rombach, Marshall Burke, David Lobell, and Stefano Ermon. Diffusionsat: A generative foundation model for satellite imagery. *arXiv preprint arXiv:2312.03606*, 2023. 1
- [16] Bo Li, Kaitao Xue, Bin Liu, and Yu-Kun Lai. Bdbm: Image-to-image translation with brownian bridge diffusion models. In *Proceedings of the IEEE/CVF conference on computer vision and pattern Recognition*, pages 1952–1961, 2023. 2, 3
- [17] Kaiyu Li, Jiawei Jiang, Andrea Codegoni, Chengxi Han, Yupeng Deng, Keyan Chen, Zhuo Zheng, Hao Chen, Zhengxia Zou, Zhenwei Shi, et al. Open-cd: A comprehensive toolbox for change detection. *arXiv preprint arXiv:2407.15317*, 2024. 7
- [18] Yuheng Li, Haotian Liu, Qingyang Wu, Fangzhou Mu, Jianwei Yang, Jianfeng Gao, Chunyuan Li, and Yong Jae Lee. Gligen: Open-set grounded text-to-image generation. In *Proceedings of the IEEE/CVF conference on computer vision and pattern recognition*, pages 22511–22521, 2023. 2
- [19] Liqin Liu, Bowen Chen, Hao Chen, Zhengxia Zou, and Zhenwei Shi. Diverse hyperspectral remote sensing image synthesis with diffusion models. *IEEE Transactions on Geoscience and Remote Sensing*, 61: 1–16, 2023. 1
- [20] Moshe Pollak and David Siegmund. A diffusion process and its applications to detecting a change in the drift of brownian motion. *Biometrika*, 72(2):267–280, 1985. 3
- [21] Alec Radford, Jong Wook Kim, Chris Hallacy, Aditya Ramesh, Gabriel Goh, Sandhini Agarwal, Girish Sastry, Amanda Askell, Pamela Mishkin, Jack Clark, et al. Learning transferable visual models from natural language supervision. In *International conference on machine learning*, pages 8748–8763. PMLR, 2021. 6
- [22] Y Ren, Y Lü, A Comber, B Fu, P Harris, and L Wu. Spatially explicit simulation of land use/land cover changes: Current coverage and future prospects. *Land Use Policy*, 80:324–336, 2019. 3
- [23] Robin Rombach, Andreas Blattmann, Dominik Lorenz, Patrick Esser, and Björn Ommer. High-resolution image synthesis with latent diffusion models. In *CVPR*, 2022. 2, 3, 6
- [24] MS Roodposhti, J Aryal, and BA Bryan. A novel algorithm for calculating transition potential in cellular automata models of land-use/cover change. *Science of the Total Environment*, 674:290–303, 2019. 3
- [25] Nataniel Ruiz, Yuanzhen Li, Varun Jampani, Yael Pritch, Michael Rubinstein, and Kfir Aberman. Dreambooth: Fine tuning text-to-image diffusion models for subject-driven generation. In *Proceedings of the IEEE/CVF conference on computer vision and pattern recognition*, pages 22500–22510, 2023. 2, 6
- [26] Tim Salimans, Ian Goodfellow, Wojciech Zaremba, Vicki Cheung, Alec Radford, and Xi Chen. Improved techniques for training gans. *Advances in neural information processing systems*, 29, 2016. 6
- [27] Hiroshi Sasaki, Chris G Willcocks, and Toby P Breckon. Unit-ddpm: Unpaired image translation with denoising diffusion probabilistic models. *arXiv preprint arXiv:2104.05358*, 2021. 2
- [28] Li Shen, Yao Lu, Hao Chen, Hao Wei, Donghai Xie, Jiabao Yue, Rui Chen, Shouye Lv, and Bitao Jiang. S2looking: A satellite side-looking dataset for building change detection. *Remote Sensing*, 13(24):5094, 2021. 5
- [29] Jiaming Song, Chenlin Meng, and Stefano Ermon. Denoising diffusion implicit models. In *ICLR*, 2021. 2
- [30] Yang Song, Jascha Sohl-Dickstein, Diederik P Kingma, Abhishek Kumar, Stefano Ermon, and Ben Poole. Score-based generative modeling through stochastic differential equations. In *ICLR*, 2021. 2, 5
- [31] Datao Tang, Xiangyong Cao, Xingsong Hou, Zhongyuan Jiang, and Deyu Meng. Crs-diff: Controllable generative remote sensing foundation model. *arXiv e-prints*, pages arXiv–2403, 2024. 1
- [32] Kai Tang and Jin Chen. Changeanywhere: Sample generation for remote sensing change detection via semantic latent diffusion model. *arXiv preprint arXiv:2404.08892*, 2024. 3
- [33] X Tong, H Liu, and Y Li. A statistical model for land use and land cover change prediction: A case study of urban growth in the beijing metropolitan area. *Environmental Modeling & Software*, 153:105418, 2022. 3

- [34] Ashish Vaswani, Noam Shazeer, Niki Parmar, Jakob Uszkoreit, Llion Jones, Aidan N Gomez, Łukasz Kaiser, and Illia Polosukhin. Attention is all you need. *Advances in neural information processing systems*, 30, 2017. 5
- [35] Ming Chen Wang and George Eugene Uhlenbeck. On the theory of the brownian motion ii. *Reviews of modern physics*, 17(2-3):323, 1945. 3
- [36] Yuxiang Wei, Yabo Zhang, Zhilong Ji, Jinfeng Bai, Lei Zhang, and Wangmeng Zuo. Elite: Encoding visual concepts into textual embeddings for customized text-to-image generation. In *Proceedings of the IEEE/CVF International Conference on Computer Vision*, pages 15943–15953, 2023. 6
- [37] Kunping Yang, Gui-Song Xia, Zicheng Liu, Bo Du, Wen Yang, Marcello Pelillo, and Liangpei Zhang. Semantic change detection with asymmetric siamese networks. *arXiv preprint arXiv:2010.05687*, 2020. 5
- [38] Yang Yang, Wen Wang, Liang Peng, Chaotian Song, Yao Chen, Hengjia Li, Xiaolong Yang, Qinglin Lu, Deng Cai, Boxi Wu, et al. Lora-composer: Leveraging low-rank adaptation for multi-concept customization in training-free diffusion models. *arXiv preprint arXiv:2403.11627*, 2024. 2
- [39] Huan Ye, Jian Zhang, Shu Liu, Xinzhu Han, and Wenjun Yang. Ip-adapter: Text compatible image prompt adapter for text-to-image diffusion models. *arXiv preprint*, arXiv:2308.06721, 2023. 6
- [40] Sihyun Yu, Kihyuk Sohn, Subin Kim, and Jinwoo Shin. Video probabilistic diffusion models in projected latent space. In *Proceedings of the IEEE/CVF conference on computer vision and pattern recognition*, pages 18456–18466, 2023. 2
- [41] Zhiping Yu, Chenyang Liu, Liqin Liu, Zhenwei Shi, and Zhengxia Zou. Metaearth: A generative foundation model for global-scale remote sensing image generation. *IEEE Transactions on Pattern Analysis and Machine Intelligence*, 2024. 1
- [42] Qi Zang, Jiayi Yang, Shuang Wang, Dong Zhao, Wenjun Yi, and Zhun Zhong. Changediff: A multi-temporal change detection data generator with flexible text prompts via diffusion model, 2024. 1, 3
- [43] Fangneng Zhan, Yingchen Yu, Kaiwen Cui, Gongjie Zhang, Shijian Lu, Jianxiong Pan, Changgong Zhang, Feiying Ma, Xuansong Xie, and Chunyan Miao. Unbalanced feature transport for exemplar-based image translation. In *Proceedings of the IEEE/CVF Conference on Computer Vision and Pattern Recognition*, pages 15028–15038, 2021. 6
- [44] Lvmin Zhang, Anyi Rao, and Maneesh Agrawala. Adding conditional control to text-to-image diffusion models. In *Proceedings of the IEEE/CVF International Conference on Computer Vision*, pages 3836–3847, 2023. 5, 6
- [45] Yuxin Zhang, Nisha Huang, Fan Tang, Haibin Huang, Chongyang Ma, Weiming Dong, and Changsheng Xu. Inversion-based style transfer with diffusion models. In *Proceedings of the IEEE/CVF Conference on Computer Vision and Pattern Recognition*, pages 10146–10156, 2023. 2
- [46] Zhuo Zheng, Ailong Ma, Liangpei Zhang, and Yanfei Zhong. Change is everywhere: Single-temporal supervised object change detection in remote sensing imagery. In *Proceedings of the IEEE/CVF International Conference on Computer Vision (ICCV)*, pages 15193–15202. IEEE, 2021. 7
- [47] Zhuo Zheng, Shiqi Tian, Ailong Ma, Liangpei Zhang, and Yanfei Zhong. Scalable multi-temporal remote sensing change data generation via simulating stochastic change process. In *Proceedings of the IEEE/CVF International Conference on Computer Vision*, pages 21818–21827, 2023. 3
- [48] Zhuo Zheng, Stefano Ermon, Dongjun Kim, Liangpei Zhang, and Yanfei Zhong. Changen2: Multi-temporal remote sensing generative change foundation model. *IEEE Transactions on Pattern Analysis and Machine Intelligence*, 2024. 1, 3
- [49] Linqi Zhou, Aaron Lou, Samar Khanna, and Stefano Ermon. Denoising diffusion bridge models. *arXiv preprint arXiv:2309.16948*, 2023. 2